Journal of
Experimental and Theoretical Analyses

MDPI

Article

Comparative Analysis of Water Hammer Performance in Different Pipe Parameters with FSI

Mostafa Kandil [1], Tamer A. El-Sayed [1,2,3,*] and Ahmed M. Kamal [1]

[1] Department of Mechanical Design, Faculty of Engineering, Mataria, Helwan University, Helmeiat-Elzaton, P.O. Box 11718 Cairo, Egypt; mustafa_abdulmutalleb@m-eng.helwan.edu.eg (M.K.); amkamalg@m-eng.helwan.edu.eg (A.M.K.)
[2] Centre for Applied Dynamics Research, School of Engineering, University of Aberdeen, Aberdeen AB24 3UE, UK
[3] School of Engineering, University of Hertfordshire Hosted by Global Academic Foundation, Cairo, Egypt
* Correspondence: tamer_alsayed@m-eng.helwan.edu.eg or tamer.el-sayed@abdn.ac.uk

Abstract: Water hammer (WH) is a critical phenomenon in fluid-filled piping systems that can lead to severe pressure surges and structural damage. The characteristics of the pipe material, geometry, and support conditions play a crucial role in the fluid–structure interaction (FSI) during WH events. This study investigates the impact of various pipe parameters, including material, length, thickness, and diameter, on the WH behavior using an FSI-based numerical approach. A comprehensive computational model was developed based on the algorithm presented in Delft Hydraulics Benchmark Problem (A) to simulate the WH phenomenon in pipes made of different materials, such as steel, copper, ductile iron, PPR (polypropylene random copolymer), and GRP (glass-reinforced plastic). This study examines the influence of pipe parameters on WH performance in pipelines, utilizing FSI to analyze the phenomenon. The results show that the pipe material has a significant influence on the pressure wave speed, stress wave propagation, and the overall system response during WH. Pipes with lower modulus of elasticity, such as PPR and GRP, exhibit lower pressure wave speeds but higher stress wave speeds compared with steel pipes. Increasing the elastic modulus, pipe wall thickness, length, and diameter enhances the pipe's stiffness and impacts the timing, magnitude of pressure surges, and the likelihood of cavitation. The findings of this study provide valuable insights into the design and mitigation of WH in piping systems.

Keywords: water hammer; fluid–structure interaction (FSI); pipeline design; pipe parameters

Citation: Kandil, M.; El-Sayed, T.A.; Kamal, A.M. Comparative Analysis of Water Hammer Performance in Different Pipe Parameters with FSI. *J. Exp. Theor. Anal.* **2024**, *2*, 58–79. https://doi.org/10.3390/jeta2030006

Academic Editor: Marco Rossi

Received: 14 May 2024
Revised: 24 July 2024
Accepted: 1 August 2024
Published: 20 August 2024

1. Introduction

Fluid–structure interaction (FSI) plays a crucial role in the dynamics of liquid-filled pipes, particularly during WH events. The interaction between the fluid and the pipe material can significantly impact the performance of the system, leading to variations in pressure and stress waves.

The method of characteristics (MOC) is a numerical method that solves the FSI equations in the time domain by transforming them into ordinary differential equations along characteristic lines. This method is particularly useful for analyzing the dynamics of fluid-filled pipes under various operating conditions, including WH events.

WH is a transient phenomenon that arises in fluid systems when a sudden change in flow rate occurs. This sudden change can be triggered by the rapid closure of a valve, the start or stop of a pump, or a change in fluid level. The resulting pressure wave propagates through the fluid system, posing a risk of damage if not properly managed. During WH, the interaction between the fluid and the tube wall is characterized by FSI. Four key variables of FSI are affected by WH: water pressure, water velocity, axial stress in the tube wall, and axial velocity in the tube wall. Figure 1 depicts two distinct waves: a fluid wave on the left

represents the wave generated by WH in the fluid, while a wave in the pipe structure on the right represents the stress wave generated by WH in the pipe wall.

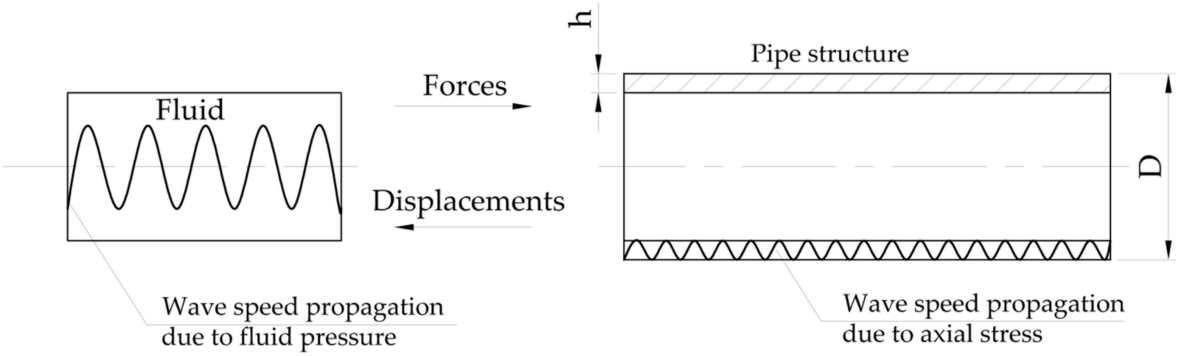

Figure 1. The propagation of wave speed in liquid and tubes during WH events [1].

For thin-walled tubes, the mass of the tubes can be neglected when analyzing the effects of WH, as the four-equation model for FSI is sufficient for examining WH on straight tubes [2].

Several studies have explored the combination of FSI with other phenomena related to wave dissipation, including the elasticity of wall tubes [3–5]. Additionally, studies have examined the phenomenon of cavitation of liquid during WH [6] and the effects of unsteady friction and viscoelasticity in tube wall structures [7].

Tijsseling and Lavooij [8] investigated the interaction between pressure surges and pipe motion, with a focus on the phenomenon of WH and fluid–structure interaction. The authors aimed to understand how pipes are affected by high pressure during water hammer, which is not accounted for in classical WH theory. Furthermore, they sought to distinguish and analyze the three interaction mechanisms—friction, Poisson, and junction coupling—and to assess their influence on extreme pressures during WH occurrences. Tijsseling [9] presented a rigorous derivation of one-dimensional equations describing FSI mechanisms in the axial/radial vibration of liquid-filled pipes, accounting for the thickness of the pipe wall through the averaging of hoop and radial stresses. The author investigated the influence of wall thickness on wave propagation speeds, natural cycles, and WH pressure waves, and compared predictions from thin- and thick-walled theories with experimental data obtained from a relatively thick pipe. The motivation for this research was the need for a more accurate understanding of WH with FSI in pipes with thick walls, which is common in practice. Zhang et al. [10] conducted an analytical investigation of WH in a hydraulic pressurized pipe system with a throttled surge chamber for slow closure. The authors aimed to derive analytical formulas for maximum WH pressures and develop a design/analysis tool for engineers and researchers, particularly in the hydropower industry. Adamkowski et al. [11] conducted an experimental investigation to examine the effects of pipeline support stiffness on WH phenomena. The authors studied the dynamic interaction between the liquid and the structure of the pipeline, focusing on the influence of elastic pipe supports on transient flow parameters and resulting WH pressures. The study also sought to provide a physical interpretation and explanation of the experimental results, enhancing the understanding of this complex phenomenon. Pezzinga et al. [12] investigated the reduction of unsteady flow oscillations in pressure pipelines by inserting in-line sections with low wave speed, specifically using additional pipes made of high-density polyethylene (HDPE) in pumping installations. The authors experimentally and theoretically evaluated the effectiveness of these additional pipes in reducing unsteady flow oscillations and assessed the mechanical parameters of the pipe material using numerical models. Furthermore, the authors sought to derive analytical solutions for frictionless pipelines with the additional pipe considered elastic, and to contribute to the design of the device for reducing unsteady flow oscillations.

In their study, Garg and Kumar [13] provided analytical solutions for frictionless pipelines with an additional elastic pipe, contributing to the design of devices for reducing unsteady flow oscillations. The authors investigated the impact of different materials and configurations on WH in pipelines, conducting experimental and numerical investigations on metallic viscoelastic pipelines under transient conditions [14]. Keramat et al. [15] presented a mathematical model and a numerical solution that considered support and elbow motion in FSI with pipe wall viscoelasticity during WH events. By incorporating both effects simultaneously, the authors derived the governing equations for hydraulics and structures, offering appropriate numerical solutions and validation from various perspectives.

Two methods for analyzing hydraulic transients using FSI to calculate transient pressure in pipeline systems were discussed [16]. The first method, known as the two-mode method, utilized the MOC-finite element method (FEM) for water and tube wall interactions. The second method, known as the full MOC method, focused on path sides [17,18]. Lavooij et al. [19] applied a two-equation model to solve FSI unknown variables such as WH pressure, water velocity, axial stress in the tube wall, and axial velocity in the tube wall.

Keramat et al. [20] developed a method for detecting leaks in pipes using transient-based techniques in the frequency domain, taking into account the interactions between the fluid and the pipe structure, and the viscoelastic properties of the pipe material. Gao et al. [21] developed a method for analyzing the frequency domain FSI vibration characteristics of aircraft hydraulic pipes with complex constraints. The study aimed to investigate the FSI behavior of these pipes under various operating conditions, including flow pulsation excitation, and to provide a comprehensive understanding of the vibration responses and their effects on the pipe's structural integrity. Li et al. [22] developed a method for analyzing the frequency domain FSI in liquid-filled pipe systems using the transfer matrix method. The study aimed to investigate the FSI behavior of these systems under various operating conditions and provide a comprehensive understanding of the vibration responses and their effects on the pipe's structural integrity.

Andrade et al. [23] investigated the FSI coupling mechanisms in liquid-filled viscoelastic pipes under the influence of fast transients. The study aimed to extend a recently developed quasi-2D flow model for fluid transients in viscoelastic pipes to handle FSI and analyze the effects of FSI on the pipe's behavior during fast transient events.

Bayle et al. [24] provided explicit analytic solutions in the Laplace domain for FSI WH waves within a pipe. The study aimed to transpose the transfer matrix method (TMM) to the equivalent two-wave propagating problem rather than applying it directly to the FSI four equations. By using the classical wave matrix diagonalization approach, the researchers could decouple wave propagation while still coupling boundary conditions in the diagonal base.

Henclik et al. [25] investigated the influence of dynamic FSI on the course of (WH) in a non-rigid pipeline system. The study focused on a specific model of FSI behavior, where a straight pipeline with a steady flow was fixed to the floor with several rigid supports and a quickly closed valve was installed at the end. The valve was attached to the pipeline with a spring/dashpot system, which allowed for dynamic energy transfer between the fluid and the structure. The research aimed to analyze the transient pressure changes in the pipeline for various stiffness and damping parameters of the spring/dashpot valve attachment. The solutions were found both analytically and numerically using a four-equation model of WH-FSI and specific boundary conditions at the valve. The study also investigated the influence of valve attachment parameters on the WH courses and found that the transient amplitudes could be reduced by optimizing these parameters.

Urbanowicz et al. [26]'s development in analytical wall shear stress modeling for water hammer phenomena was to enhance the understanding and prediction of wall shear stress effects during water hammer events in fluid systems. By advancing analytical models for calculating wall shear stress, the study aimed to improve the accuracy and reliability of simulations, thereby enabling better assessment of the impact of WH on pipeline integrity, flow stability, and system efficiency. The research contributed to the development of more

comprehensive and effective strategies for mitigating the adverse effects of WH in industrial and municipal piping systems.

Covas et al. investigated the complex interplay between viscoelastic behavior of pipe walls, unsteady friction, and transient pressures in piping systems. The research aimed to develop numerical models and simulations to understand the effects of viscoelasticity and unsteady friction on transient flow behavior, particularly WH in viscoelastic pipes [27]. Yazdi et al. [28] presented a new modeling to improve WH metamodeling techniques such as artificial neural network (ANN), support vector regression (SVR), and adaptive neuro-fuzzy inference system (ANFIS). Results showed that ANN was the most accurate, followed by ANFIS, while SVR had lower generalization capability. To determine the best size and location for WH control devices in a pipeline, researchers used a combination of ANN and differential evolution (DE).

Hyunjun and Kim [29] developed a more advanced quasi-2D model for transient events inducing cavitation in flow. The model aimed to provide a more comprehensive understanding of the complex interactions between cavitation and WH effects in a reservoir/pipeline/valve system. By incorporating the density of the liquid–vapor mixture, considering radial flux, and utilizing a hybrid solution scheme, the authors aimed to improve the accuracy and reliability of simulations for transient events with cavitation. The ultimate goal of the research was to contribute to the advancement of hydraulic analysis and the management of pipeline systems by providing a more effective model for predicting mass transport and ensuring system safety. Triki et al. [30] introduced and developed an innovative "compound technique" for in-line water hammer control in steel pressurized-piping systems. The authors aimed to overcome the limitations of the conventional inline strategy by combining the benefits of different polymeric material types and optimizing the design strategy for improved performance. This approach enhanced the control of water hammer in pressurized pipe flow by addressing the drawbacks of the primitive implementation technique. Kandil et al. [31] employed an analytical model to investigate the influence of various tube materials on WH phenomena. The study revealed that the selection of pipe materials for conveying liquids had a substantial impact on the WH reaction.

Skalak [32] expanded upon the existing theory of WH, providing a more comprehensive solution that included several novel features not present in the elementary theory. The author re-examined the existing theory and analyzed the propagation of pressure waves in a cylindrical tube filled with an elastic fluid. The research aimed to enhance the understanding of WH and improve the accuracy of predictions related to pressure waves in fluid-filled tubes introduced by Joukovsky in his classical theory [33].

Chaudhry [34] analyzed and modeled the behavior of pressure transients, particularly WH, in piping systems. The author aimed to develop numerical models and simulations to understand the effects of various factors, including viscoelasticity, unsteady friction, and transient pressures, on the behavior of pressure transients in piping systems. The research aimed to provide practical insights into the design and operation of piping systems, focusing on mitigating the negative effects of pressure transients on the system. Ferras et al. [35] investigated the impact of FSI during hydraulic transients in pipe coils, developing mathematical models, numerically implementing them, and validating them with experimental evidence. The goal was to create a comprehensive model that captured the behavior of pipes during hydraulic transients, incorporating both axial stress waves in the pipe wall and fluid conservation principles.

Watters [36] examined the behavior of PVC pipes under the influence of WH pressure waves, questioning the validity of applying the classical theory of hydraulic transients to these pipes. The study was prompted by the growing use of plastic materials, particularly PVC, in constructing water pipes and the need for a deeper understanding of their behavior under WH conditions. The research aimed to provide insights into the extent to which the classical theory of hydraulic transients accurately predicts WH in PVC pipes and to identify any discrepancies between theoretical predictions and actual behavior.

Kubrak et al. [37] examined the behavior of WH in steel/plastic pipes connected in series, analyzing the effects of various steel/plastic configurations on the system. The study aimed to provide insights into the following aspects: performing WH tests for different lengths of steel and HDPE sections, considering six different steel/plastic configurations; examining how unsteady friction and the viscoelastic properties of polymer pipes affect the system. They used a WH solver and numerical calculations to simulate the behavior of the system. They compared their results with the classical theory of hydraulic transients to assess the accuracy and applicability of the theory to steel/plastic pipes connected in series. Their work showed the complex interplay between steel and plastic pipes, and the effects of unsteady friction and transient pressures in piping systems, with a focus on mitigating the negative effects of pressure transients on the system.

Kriaa et al. [38] examined the effectiveness of using rubber bypass tubes in reducing WH effects in uPVC pipes. The study focused on the following aspects: experimentally demonstrating the reduction of WH effects in uPVC pipes using rubber bypass tubes; investigating the underlying mechanisms responsible for the reduction of WH effects, including the damping properties of rubber materials and the role of rubber in attenuating pressure surges; assessing the feasibility and practical implications of implementing rubber bypass tubes in uPVC pipes for WH control, considering factors such as cost-effectiveness, ease of installation, and long-term performance. The research provided insights into the potential of rubber bypass tubes in mitigating WH effects in uPVC pipes, with a focus on the practical implications for the design and operation of piping systems.

The present study aims to investigate the comparative performance of waterways in different pipe parameters including materials, pipe wall thickness, length, and diameter using FSI. The materials used in this analysis are steel, copper, ductile iron, PPR (polypropylene random copolymer), and GRP (glass-reinforced plastic). This study employs the method of characteristics (MOC) to analyze the FSI effects in each parameter. The results provide valuable insights into the performance of each pipe parameter under WH conditions, highlighting the importance of material selection in mitigating FSI effects. This study is structured as follows: Section 2 presents the theory used in the WH model. Section 3 verifies the accuracy of the MATLAB model used in this study. Section 4 presents the analytical solution of WH equations. Section 5 presents and analyzes the numerical results obtained for different pipe materials. Section 6 summarizes the key findings and recommendations.

2. Theory and Modeling

Lavooij and Tijsseling developed a one-dimensional non-dispersive four-equation model [18], which was employed in this study to incorporate various coupling mechanisms, including Poisson coupling, junction coupling, and friction coupling.

The authors utilized MOC—a well-established technique for solving hyperbolic partial differential equations—to analyze WH phenomena in pipe systems. This method is commonly used to obtain exact or approximate solutions for hyperbolic PDE systems, as detailed in the references [39].

The four-equation model (Equations (1)–(4)) for FSI in WH problems is a fundamental framework for analyzing the transient behavior of pressurized pipe flows. The model consists of four hyperbolic equations that describe the fluid motion, fluid continuity, and structural dynamics. The first equation represents the fluid motion, which is governed by the Navier–Stokes equation. The second equation ensures mass conservation by describing the fluid continuity. The third equation accounts for the structural dynamics, including the effects of pipe stiffness and damping. The fourth equation represents the interaction between the fluid and the structure, capturing the effects of fluid–structure coupling. These four equations form the core of the FSI model.

$$\frac{\partial V}{\partial t} + \frac{1}{\rho_l}\frac{\partial p}{\partial z} = 0 \tag{1}$$

$$\frac{\partial V}{\partial z} + \left(\frac{1}{K} + \frac{2R}{Eh}\right)\frac{\partial p}{\partial t} - 2v\frac{\partial U}{\partial Z} = 0 \tag{2}$$

$$\frac{\partial U}{\partial t} - \frac{1}{\rho_t}\frac{\partial \sigma}{\partial z} = 0 \tag{3}$$

$$\frac{\partial U}{\partial z} - \frac{1}{E}\frac{\partial \sigma}{\partial t} + \frac{Rv}{hE}\frac{\partial p}{\partial t} = 0 \tag{4}$$

$$a^2 = \left[\frac{\rho_l}{K} + \frac{2\rho_l R}{hE}\right]^{-1}, c^2 = \frac{E}{\rho_t} \tag{5}$$

The variables used in the analysis of WH phenomena in pipelines are as follows: axial tube velocity (U), velocity of liquid (V), time (t), classical pressure wave speed in the water (a), axial stress wave speeds (c), liquid cross-sectional area (A_l), tube cross-sectional area (A_t), modulus of electricity (E), thickness of tube wall (h), gravity acceleration (g), tube Poisson ratio (v), inner radius of the tube (R), liquid density (ρ_l), tube density (ρ_t), liquid bulk modulus (K), time (t), Cartesian coordinate system axis (z), axial stress in tube wall (σ), and liquid transient pressure (p). The analysis focused on the WH caused by the instantaneous closure of the valve in the tank/tube/valve system, as depicted in Figure 2.

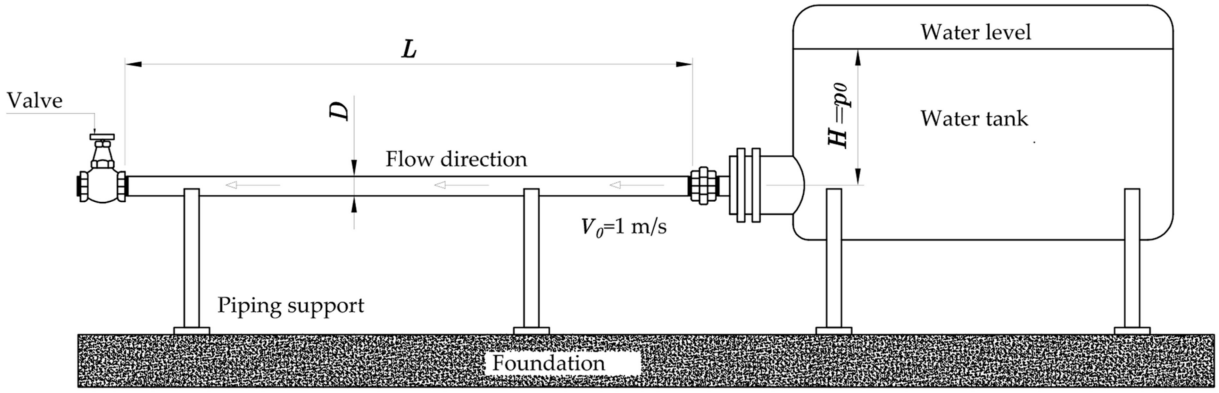

Figure 2. The Benchmark Problem (A) pipeline model comprises a system of valves, pipes, and a tank.

3. Model Verification

This paper builds upon the same model and algorithms presented in [40] and includes a custom-developed MATLAB code tailored to this specific study. In this section, the results obtained from the computer program are compared to those presented in [40] using identical variables.

The Delft Hydraulics Benchmark Problem A is a widely recognized test case used to evaluate numerical methods and FSI models [8]. It consists of a tank/tube/valve system with specific geometric and material properties, as shown in Figure 2. The problem is defined by parameters such as tube length, radius, wall thickness, material properties, and fluid velocity. The benchmark problem is characterized by the wave speeds and their ratio, which are essential for assessing the performance of numerical methods and FSI models. It serves as a standard test case for validating and comparing different approaches to simulating WH and FSI phenomena. The Delft Hydraulics Benchmark A has been extensively used in the research community to advance the understanding and modeling of WH and FSI in pipeline systems [40].

The results obtained from the program developed for this study were validated against the Delft Hydraulics Benchmark A, a well-established benchmark case for FSI in WH analysis. As shown in Figure 3, the pressure profiles generated by the used MATLAB program closely match the reference data from the Delft Hydraulics Benchmark A. This

alignment demonstrates the accuracy and reliability of the used MATLAB numerical model in capturing the complex FSI phenomena occurring in the pipeline system. The ability to replicate the benchmark results provides confidence in the applicability of the used MATLAB program to analyze WH events in a variety of pipe materials and configurations. This validation step ensures that the insights and conclusions drawn from comparative analysis of different pipe materials are grounded in a robust and well-tested numerical framework, further strengthening the overall quality and credibility of this research.

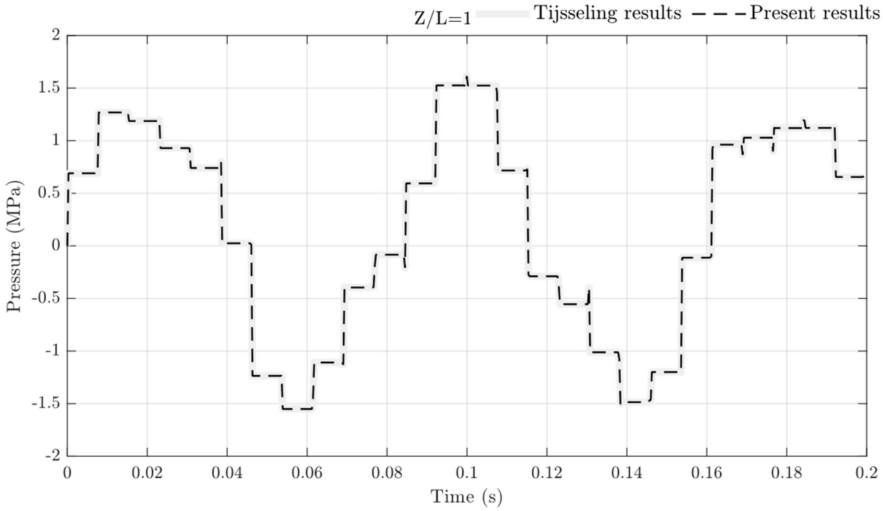

Figure 3. Verification of proposed MATLAB program with Benchmark Problem (A) for a freely moving valve ($Z/L = 1$) with reference to absolute pressure.

Table 1 presents the complete characteristics of the Benchmark Problem A parameters. It is crucial to note that the dimensions specified are adopted from [40] and that the validation is based solely on numerical data.

Table 1. Benchmark Problem (A) parameters.

Parameters	**Benchmark Problem (A)**
Tube length (**L**)	20 m
Tube inner radius (***R***)	398.5 mm
Tube wall thickness (**h**)	8 mm
Modulus of elasticity (**E**)	210 GPa
Water bulk modulus (**K**)	2.1 GPa
Water initial flow velocity ($\mathbf{V_o}$)	1 m/s
Density of water ($\boldsymbol{\rho_l}$)	1000 Kg/m^3
Density of tube ($\boldsymbol{\rho_t}$)	7900 Kg/m^3
Tube Poisson ratio	0.3
Pressure behind valve	0 Pa
Intial pressure (reservoir head) ($\boldsymbol{p_o}$)	1 bar
Pressure wave speeds ($\boldsymbol{\eta_1}$ & $\boldsymbol{\eta_2}$)	$\pm$1024.7 m/s
Stress wave speeds ($\boldsymbol{\eta_3}$ & $\boldsymbol{\eta_4}$)	$\pm$5280.5 m/s
Valve closure time	0.02 s

To investigate the WH phenomenon in the proposed model, the four system dependent variables (WH pressure, water velocity (V), axial tube velocity (U), and axial stress in tube wall (σ)) are calculated at four locations along the tube length, and the results are examined. "Z" is the distance from the main supply header along the tube and "L" is the total pipe length.

4. Analytical Solution of WH Equations

It is assumed that the acoustic phenomenon during the WH being studied can be represented with the following set of equations.

$$\mathbf{A}\frac{\partial}{\partial t}\boldsymbol{\phi}(z,t) + \mathbf{B}\frac{\partial}{\partial z}\boldsymbol{\phi}(z,t) + \mathbf{C}\boldsymbol{\phi}(z,t) = 0 \tag{6}$$

Constant matrices **A** and **B** are invertible, and $\mathbf{A^{-1}B}$ is diagonalizable. Constant matrix **C**, which, when singular, causes frequency dispersion (if $\mathbf{C} \neq 0$). N dependent variables ϕ_i—constituting the state vector ϕ—are functions of the independent variables z (space) and t (time), considering N = 4 and **C** = 0.

In Equation (6), the axial vibration of a liquid-filled tube (Equations (1)–(4)) can be depicted using a state vector.

$$\boldsymbol{\phi} = \begin{Bmatrix} V \\ p \\ U \\ \sigma \end{Bmatrix} \tag{7}$$

The coefficients' matrices

$$\mathbf{A} = \begin{bmatrix} 1 & 0 & 0 & 0 \\ 0 & \left(\rho_l a^2\right)^{-1} & 0 & 0 \\ 0 & 0 & 1 & 0 \\ 0 & vR(Eh)^{-1} & 0 & -\left(\rho_t c^2\right)^{-1} \end{bmatrix} \tag{8}$$

$$\mathbf{B} = \begin{bmatrix} 0 & {\rho_l}^{-1} & 0 & 0 \\ 1 & 0 & -2v & 0 \\ 0 & 0 & 0 & -{\rho_t}^{-1} \\ 0 & 0 & 1 & 0 \end{bmatrix} \tag{9}$$

The characteristic equation

$$|\mathbf{B} - \boldsymbol{\eta}\mathbf{A}| = \mathbf{0} \tag{10}$$

In Appendix A, it is shown that characteristic equation $|\mathbf{B} - \boldsymbol{\eta}\mathbf{A}| = 0$ has four distinct real roots, indicating that matrix $\mathbf{A^{-1}}$ **B** also possesses four distinct real eigenvalues. These four characteristic roots or eigenvalues signify $\boldsymbol{\eta_i}$.

Equation (6) is referred to in hyperbolic form. In this instance, it can be converted into a more convenient form by multiplying it with a regular matrix **T**.

$$\mathbf{TA}\frac{\partial}{\partial t}\boldsymbol{\phi}(z,t) + \mathbf{TB}\frac{\partial}{\partial z}\boldsymbol{\phi}(z,t) = 0 \tag{11}$$

Based on the principles of linear algebra, it is established that, for any square matrix with unique real eigenvalues, denoted as $\mathbf{A^{-1}B}$, there is a corresponding matrix **S** such that

$$\mathbf{S}^{-1}\mathbf{A}^{-1}\mathbf{BS} = \Delta \tag{12}$$

where Δ is diagonal:

$$\Delta = \begin{bmatrix} \boldsymbol{\eta_1} & 0 & 0 & 0 \\ 0 & \boldsymbol{\eta_2} & 0 & 0 \\ 0 & 0 & \boldsymbol{\eta_3} & 0 \\ 0 & 0 & 0 & \boldsymbol{\eta_4} \end{bmatrix} \tag{13}$$

By considering matrix **T** as the following:

$$\mathbf{T} = \mathbf{S}^{-1}\mathbf{A}^{-1} \tag{14}$$

Substitution of (14) into (12)

$$\mathbf{TB} = \Delta\ \mathbf{T}\ \mathbf{A} \tag{15}$$

Substitution of (15) into (11)

$$\mathbf{TA}\frac{\partial}{\partial t}\boldsymbol{\phi}(z,t) + \Delta\ \mathbf{T}\ \mathbf{A}\frac{\partial}{\partial z}\boldsymbol{\phi}(z,t) = 0 \tag{16}$$

Equation (16) is commonly referred to as the standard form of system (11). Introduction of the vector

$$\boldsymbol{v}\ =\ \mathbf{T}\ \mathbf{A}\ \boldsymbol{\phi}(z,t) \tag{17}$$

Substitution of (17) into (16)

$$\frac{\partial \boldsymbol{v}}{\partial t} + \Delta\ \frac{\partial \boldsymbol{v}}{\partial z} = 0 \tag{18}$$

Equation (18) can be simplified to the following:

$$\frac{\partial v_i}{\partial t} + \eta_i\ \frac{\partial v_i}{\partial z} = 0,\ i = 1,\ 2,\ 3,\ 4 \tag{19}$$

where $\boldsymbol{\eta}$ is the eigenvalue.

Hence, the total derivative is given as

$$\frac{\mathrm{d}v_i(z,t)}{\mathrm{d}t} = 0 \tag{20}$$

$$\text{along}\ \frac{\mathrm{d}z}{\mathrm{d}t} = \eta_i \tag{21}$$

The solution to ordinary differential Equations (20) and (21) is:

$$v_i(z,t) = v_i(z - \eta_i \Delta t, t - \Delta t) \tag{22}$$

When a numerical time step Δt is utilized, or, more generally, according to Figure 4,

$$v_i(P) = v_i(A_i)\ \text{or}\ \boldsymbol{v}(P) = \begin{bmatrix} v_1(A_1) \\ v_2(A_2) \\ v_3(A_3) \\ v_4(A_4) \end{bmatrix} \tag{23}$$

The value of the unknown variable $\boldsymbol{\eta}$ does not change along the line A_i P, as shown in Figure 4:

Characteristic Equation (10), corresponding to matrices (8) and (9), is

$$\eta^4 - \mathrm{q}^2\eta^2 + a^2c^2 = 0 \tag{24}$$

where $q^2 = \left(1 + 2v^2 \frac{\rho_l}{\rho_t} \frac{R}{h}\right) a^2 + c^2$

$$\eta_1 = \frac{1}{2}\left[q^2 - \left(q^4 - 4a^2c^2\right)^{1/2}\right]^{1/2} = \hat{a} \tag{25}$$

$$\eta_2 = -\eta_1 = -\hat{a} \tag{26}$$

$$\eta_3 = \frac{1}{2}\left[q^2 + \left(q^4 - 4a^2c^2\right)^{1/2}\right]^{1/2} = \hat{c} \tag{27}$$

$$\eta_4 = -\eta_3 = -\hat{c} \tag{28}$$

In the $z-t$ plane, P and A_i are points, as depicted in Figure 4. The integrated compatibility Equations (12)–(15) reveal that for point P not on a boundary, the unknowns V, p, U, and σ are entirely determined by their values in the "upstream" points A_i. Therefore, if the boundaries are disregarded, the solution of system (11) at any point P can be derived from Equations (12)–(15), provided that initial values for V, P, U, and σ in P are known.

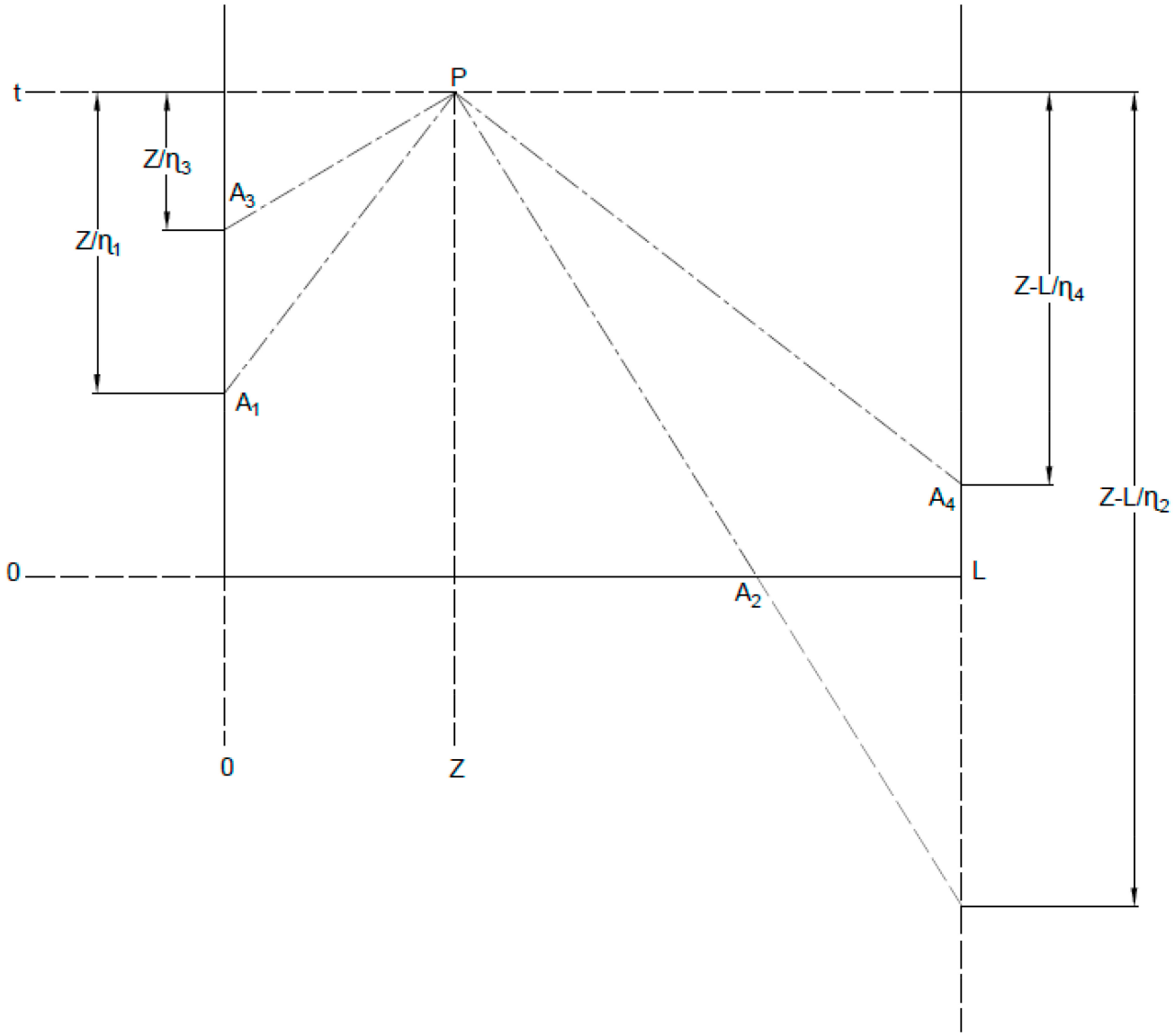

Figure 4. Point P and lines characterizing "feeding" in the distance–time plane. Reprinted with permission from [40] © Elsevier.

Determining the variables' values at known point (P) on the computational grid depicted in Figure 4 uses the data from the previous points.

The MATLAB program is used to solve the prementioned mathematical equations, and the outcomes are shown in the following Section 5.

Initial and Boundary Conditions

To simulate WH with FSI, it is essential to define the initial conditions of pressure and velocity of the water in the tube, and the initial position and deformation of the structure (e.g., tube or valve) interacting with the water. In the FSI simulation, the interaction between the water and the tube is accounted for in the boundary conditions, which include the transmission of forces and displacements at the interface between the fluid and structure.

In this study, it is assumed that the pipe system filled with liquid is initially in a state of equilibrium (steady state) before the occurrence of a transient event. The initial values of key variables, including pressure, velocity, and tube displacement, are calculated using one-dimensional equations.

In turbulent tube flow, the pressure loss (Δp_0) across a fully open valve is given by the orifice equation [35].

$$\Delta p_0 = \aleph_0 \frac{1}{2} \rho_l (V_0 - U_0)|V_0 - U_0| \tag{29}$$

where $\aleph_0$ represents an empirical loss coefficient. It is assumed that the same relation holds for a closing valve [35].

$$\Delta p = \aleph \frac{1}{2} \rho_l (V - U)|V - U| \tag{30}$$

where $\aleph$ depends on the valve position and therefore on time. Dividing Equation (29) by Equation (30) yields the dimensionless valve closure coefficient $\tau = \sqrt{\aleph_0 / \aleph}$ and the nonlinear boundary condition

$$p_o (V - U)|V - U| = \tau^2(t)(V_0 - U_0)|V_0 - U_0|\, p \tag{31}$$

Quadratic Equation (31) is solved concurrently with three linear equations (two Riemann invariants and one boundary condition) [36].

The initial conditions are used for the water and the tube in the analysis as follows:

$$V = V_0 = 1 \text{ m/s} \tag{32}$$

$$p = p_o = 1 \text{ bar} \tag{33}$$

$$U = U_0 = 0 \text{ m/s} \tag{34}$$

$$\sigma = A_l p_o / A_t \tag{35}$$

5. Results and Discussion

This study investigated the impact of various pipe parameters, including material, length, thickness, and diameter, on WH behavior using an FSI-based numerical approach. All the pipe materials examined were considered within their elastic zones. The results show that pipe material significantly influences pressure wave speed, stress wave propagation, and the overall system response during WH events. This study underscores the importance of considering pipe parameters in the design and mitigation of WH in piping systems, as changes in these parameters can significantly affect the timing and magnitude of pressure surges and the likelihood of cavitation.

5.1. Effect of Changing the Pipeline Material

The magnitude and propagation of WH pressure waves are strongly influenced by the properties of the pipe material and the FSI between the pipe wall and the flowing liquid. The pipe material affects the wave speed, which determines the timing and magnitude of the pressure surges and the potential for cavitation and pipe failure.

Previous studies have investigated the effect of pipe material on WH using various analytical and numerical approaches. However, most of these studies have focused on a limited number of pipe materials, such as steel and plastic, and have not provided a comprehensive comparison of the WH behavior across a wide range of pipe materials commonly used in engineering applications.

This research aims to investigate the impact of various pipe materials, including steel, copper, ductile iron, PPR (polypropylene random copolymer), and GRP (glass-reinforced plastic), on the WH phenomenon with FSI.

Table 2 presents the various pipe material properties that are relevant to the problem scenario involving a tank/tube/valve system, as illustrated in Figure 2.

Table 2. Mechanical properties of the pipes used in the numerical analysis [41].

Tube Material	Tube Modules of Elasticity (GPa)	Density of Tube (ρ_t) (kg/m^3)	Poisson's Ratio
Steel tube (ST)	210	7900	0.30
Copper (CU)	110	8900	0.36
Polypropylene random copolymer (PPR)	0.850	909	0.36
Ductile iron (DI)	170	7050	0.27
Glass fiber-reinforced plastic (GRP E "glass")	4.27	2100	0.30

All other dimensions and properties, including tube radius, thickness, length, and water density, are kept constant for all materials, as specified in Table 1.

Figures 5–8 presents the transient WH pressure distributions at four distinct locations along the pipeline (1/4 L, 1/2 L, 3/4 L, and total L), showcasing the variation of WH pressure, water flow velocity, axial tube velocity, and axial stress in the tube wall over time for five different pipe materials (steel (ST), copper, polypropylene (PPR), ductile iron, and glass-reinforced plastic (GRP)). The figures visually depict the variables at four locations for each material. The comparison between materials is based on the maximum value and the number of fundamental wave frequencies occurring within a 1 s time frame, as listed in Table 3.

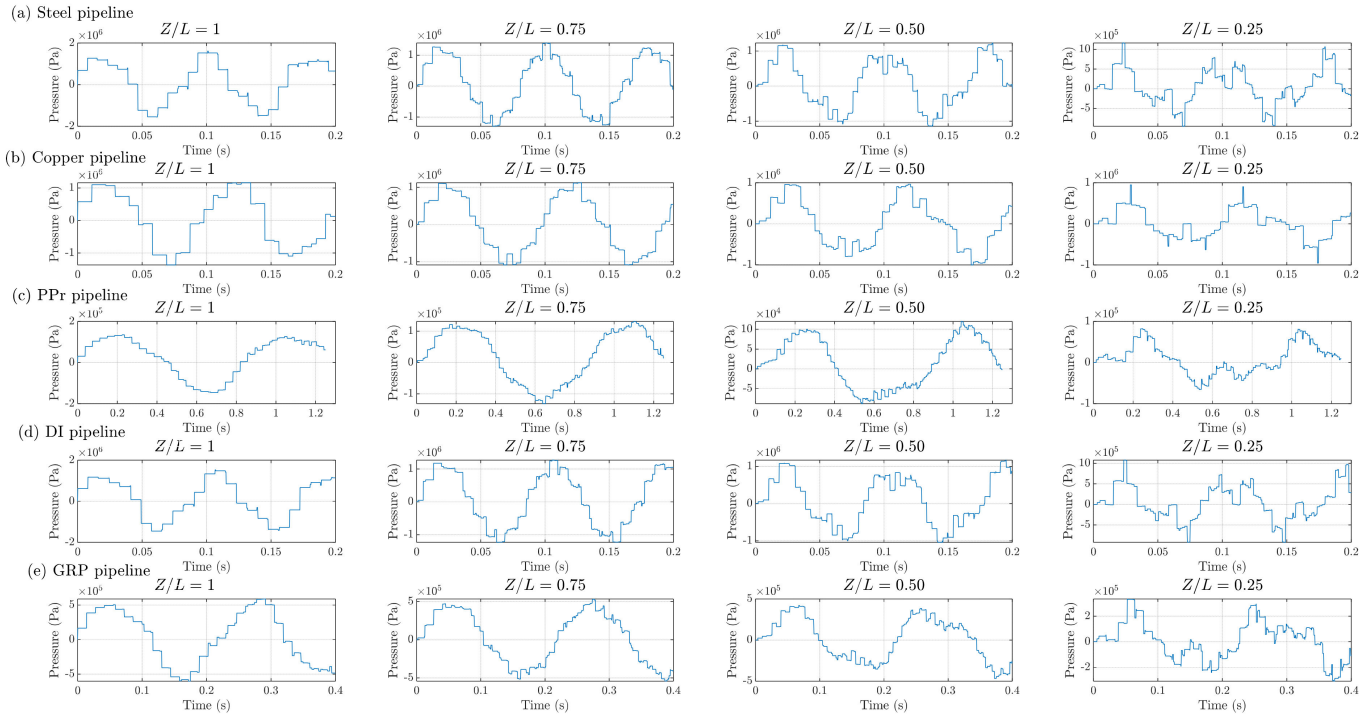

Figure 5. Results of transient pressures at four specific locations: (**a**) steel (ST), (**b**) copper (Cu), (**c**) polypropylene random copolymer (PPR), (**d**) ductile iron (DI), and (**e**) glass-reinforced plastic (GRP) pipelines.

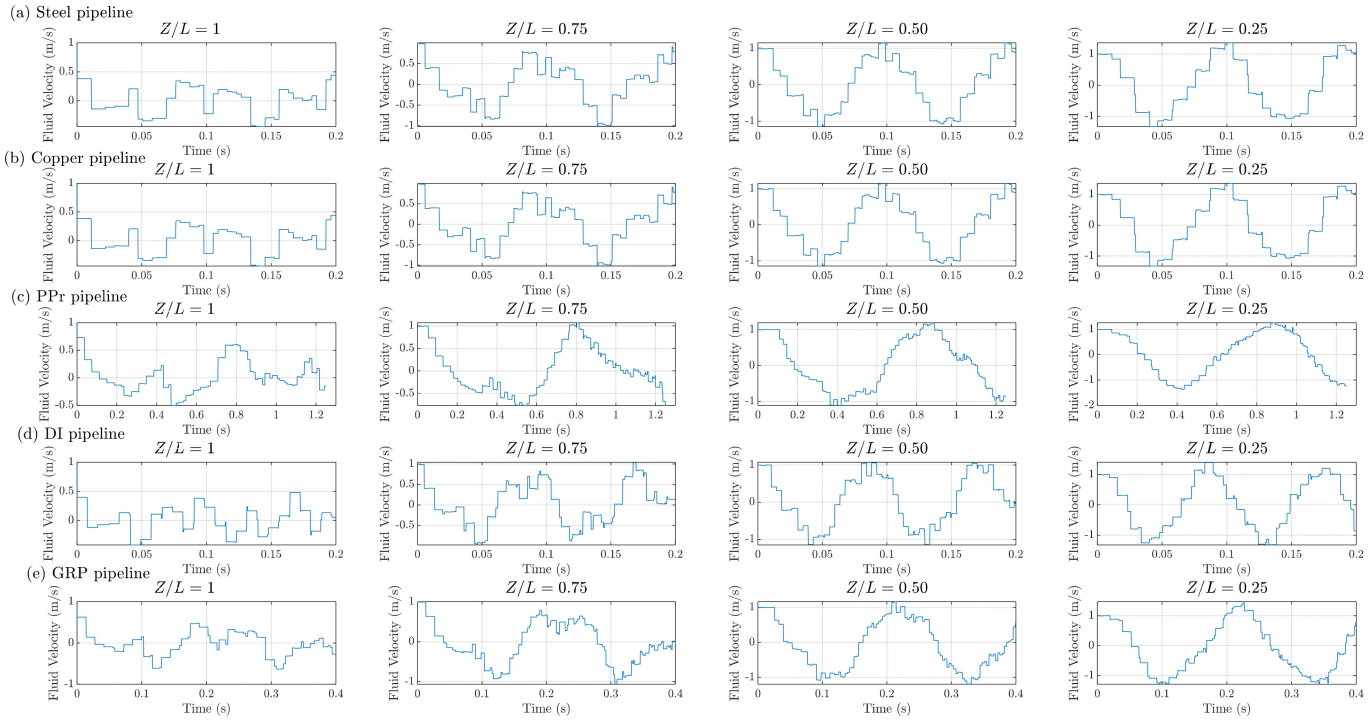

Figure 6. Results of fluid velocity at four specific locations: (**a**) steel (ST), (**b**) copper (Cu), (**c**) polypropylene random copolymer (PPR), (**d**) ductile iron (DI), and (**e**) glass-reinforced plastic (GRP) pipelines.

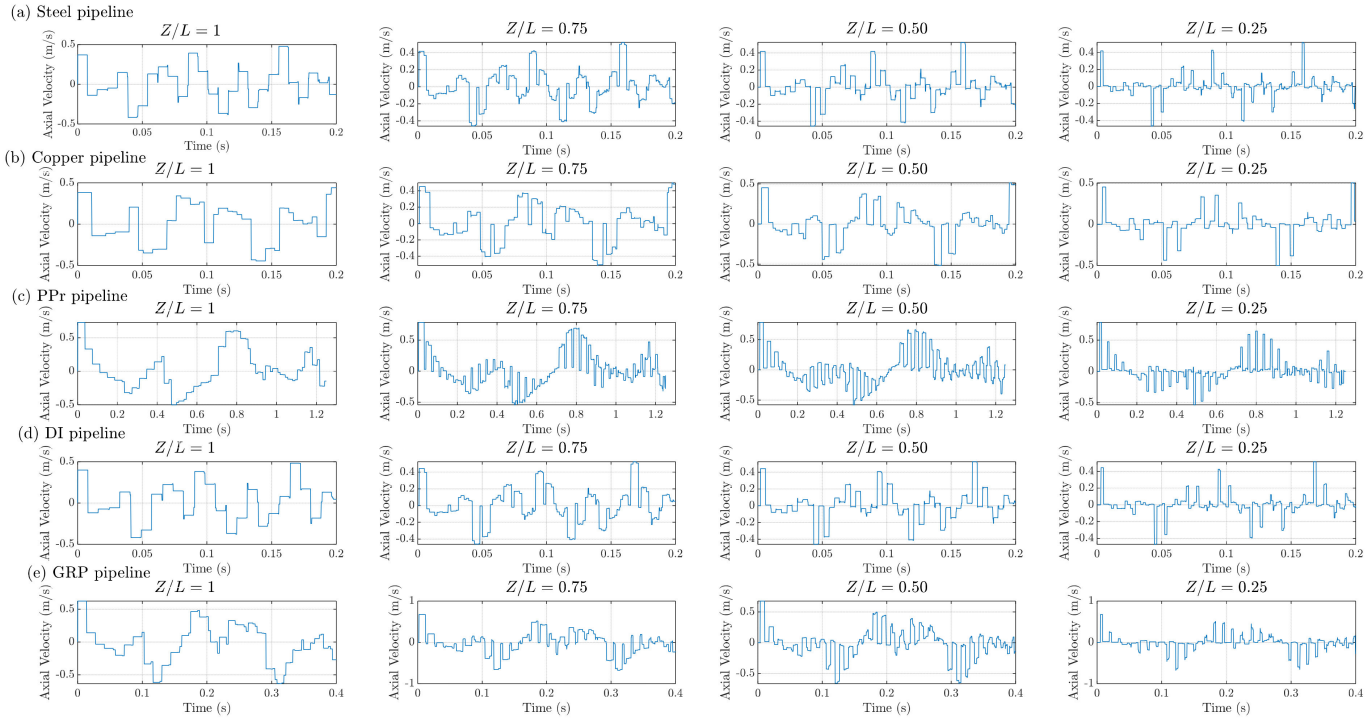

Figure 7. Results of axial tube velocity at four specific locations: (**a**) steel (ST), (**b**) copper (Cu), (**c**) polypropylene random copolymer (PPR), (**d**) ductile iron (DI), and (**e**) glass-reinforced plastic (GRP) pipelines.

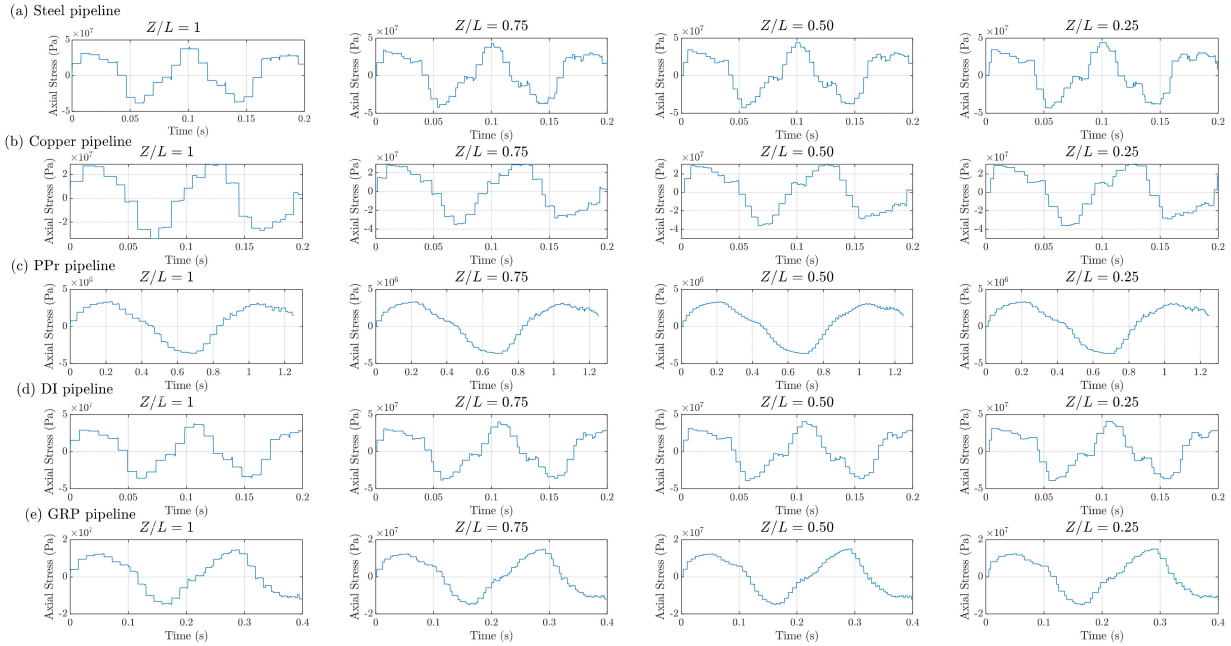

Figure 8. Results of axial stress wave in the tube wall at four specific locations: (**a**) steel (ST), (**b**) copper (Cu), (**c**) polypropylene random copolymer (PPR), (**d**) ductile iron (DI), and (**e**) glass-reinforced plastic (GRP) pipelines.

Figure 9 shows the fast Fourier transform (FFT) results for the numerical simulations of water hammer events in different types of pipeline materials at a location of $Z/L = 0.5$, where Z represents the distance along the pipeline length L. The five subfigures (a) through (e) present the FFT results for steel (ST), copper (Cu), polypropylene random copolymer (PPR), ductile iron (DI), and glass-reinforced plastic (GRP) pipelines, respectively. The FFT analysis allows for the identification of the dominant frequencies present in the WH pressure oscillations for each pipeline material.

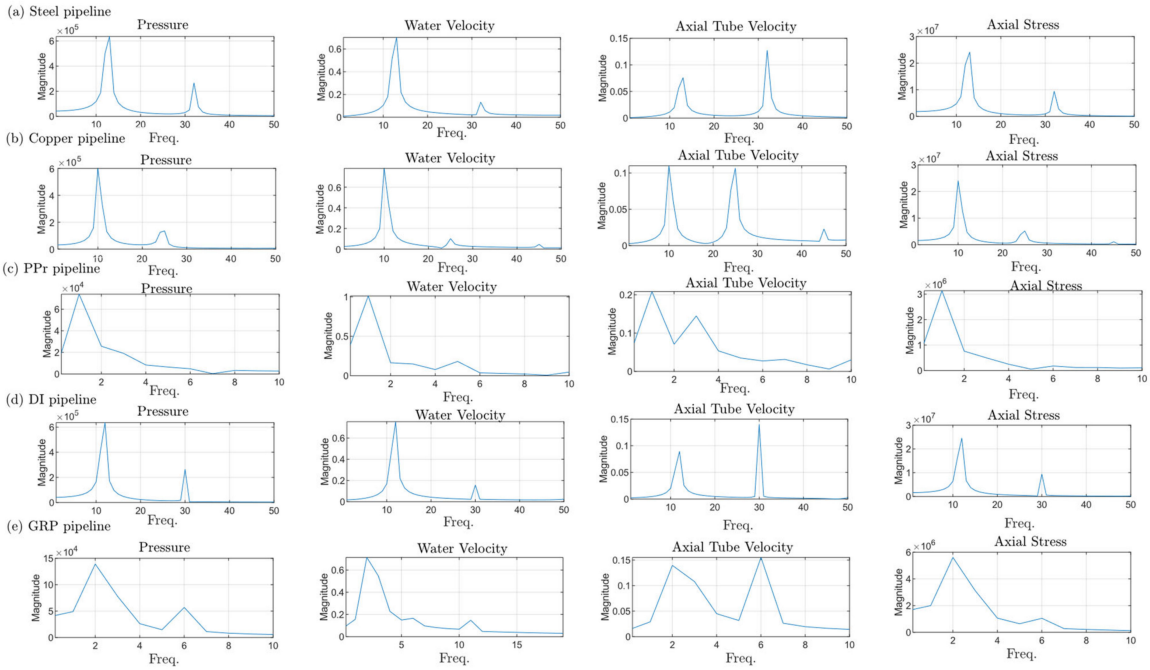

Figure 9. FFT results for numerical results at Z/L = 0.5: (**a**) steel (ST), (**b**) copper (Cu), (**c**) polypropylene random copolymer (PPR), (**d**) ductile iron (DI), and (**e**) glass-reinforced plastic (GRP) pipelines.

Table 3. Summarized WH pressure results for the five tube materials.

Tube Material	Maximum WH Pressure (MPa)	Maximum Water Flow Velocity (m/s)	Maximum Axial Tube Velocity (m/s)	Maximum Axial Stress in Tube Wall (MPa)	Fundamental Wave Frequency
Steel (ST)	1.686	0.477	0.477	41.57	13
Copper (Cu)	1.335	0.55	0.55	32.88	10
Polypropylene Random Copolymer (PPR)	0.149	0.65	0.65	3.27	1
Ductile iron (DI)	1.475	0.48	0.48	36.64	12
Glass fiber-reinforced plastic (GRP E "glass")	0.579	0.56	0.56	14.378	2

As shown in Figure 5, the results indicate that steel (ST), ductile iron, and copper exhibit higher maximum pressure values and frequencies compared with PPR and GRP. This suggests that they are less affected by WH due to the higher WH pressure over a certain number of cycles compared with PPR and GRP tube materials under the same operating conditions. Conversely, PPR displays a lower maximum pressure and fewer cycles, potentially indicating a different response to WH and suggesting a greater effect on it.

As shown in Figure 6, the results indicate that steel (ST), ductile iron, GRP, and copper exhibit lower maximum water flow velocity values compared with PPR. This suggests that they are more susceptible to WH due to the lower WH water flow velocity compared with the PPR tube material under the same operating conditions. Conversely, PPR displays a higher maximum water flow velocity and relatively low cycles.

As shown in Figure 7, the results indicate that steel (ST), ductile iron, GRP, and copper exhibit lower maximum axial tube velocity values compared with PPR. This suggests that they are more susceptible to WH due to the lower WH axial tube velocity compared with the PPR tube material under the same operating conditions. Conversely, PPR displays a higher maximum water axial tube velocity and relatively low cycles. Notably, the maximum values of water flow velocity are equivalent to the maximum axial tube velocity.

As shown in Figure 8, the results indicate that steel, ductile iron, and copper exhibit higher maximum axial stress in the tube wall values and frequencies compared with PPR and GRP. This suggests that they are less affected by WH due to the higher WH pressure and number of cycles compared with PPR and GRP tube materials under the same operating conditions. Conversely, PPR displays a lower maximum axial stress in the tube wall and has relatively low cycles, indicating a greater susceptibility to WH.

The FSI model for WH in five pipe materials (steel, copper, DI, PPR, and GRP) was analyzed to provide a more comprehensive understanding of the phenomenon. The results show that the pressure wave speed and natural frequencies of the pipes decrease as the stiffness and density of the pipe material decrease.

The wave speeds in the liquid and pipe wall during a WH event vary significantly depending on the pipe material used, as listed in Table 4.

The key observations from these data are that the wave speed in the pipe wall is significantly higher than the wave speed in the liquid for all the pipe materials. This difference in wave speeds can lead to complex fluid–structure interactions during WH events. The wave speed in the liquid is relatively consistent across the different pipe materials, ranging from around 1020 m/s for steel to 71 m/s for GRP. This is due to the similar density and bulk modulus of the liquid (water) in all cases. The wave speed in the pipe wall varies much more widely, from around 5280 m/s for steel to 510 m/s for GRP. This is due to the significant differences in the elastic modulus and density of the pipe materials.

Table 4. WH wave speeds for the five tube materials.

Tube Material	Pressure Wave Speeds (η_1 & η_2) (m/s)	Stress Wave Speeds (η_3 & η_4) (m/s)
Steel (ST)	±1024	±5280
Copper (Cu)	±848	±3660
Polypropylene random copolymer (PPR)	±92	±1070
Ductile iron (DI)	±969	±5020
Glass fiber-reinforced plastic (GRP E "glass")	±71	±510

The lower wave speeds in the PPR and GRP pipes indicate that these materials may be more susceptible to WH effects, as the pressure waves can propagate more slowly through the system. This could lead to higher pressure surges and increased risk of pipe damage or failure. In summary, the choice of pipe material has a profound impact on the wave speeds and, consequently, the WH behavior in a piping system. Understanding these material-dependent wave speed characteristics is crucial for the proper design and mitigation of WH effects.

These analyses and results provide a more comprehensive understanding of the FSI model for WH in five pipe materials. The results show that the pressure wave speed and natural frequencies of the pipes decrease as the stiffness and density of the pipe material decrease.

5.2. Effect of Changing the Pipeline Length

This study investigates the impact of pipe length on the WH behavior in steel pipes using an FSI-based numerical approach. This study considers steel pipes with lengths of 10 m, 20 m, and 30 m to analyze the effect of pipe length on the WH phenomenon. All other dimensions and properties, including tube radius, thickness, and water density, are kept constant for all materials, as specified in Table 1.

Figure 10 presents the variation of WH pressure, water flow velocity, axial tube velocity, and axial stress in the tube wall over time for the steel pipeline for pipe lengths of 10 m, 20 m, and 30 m.

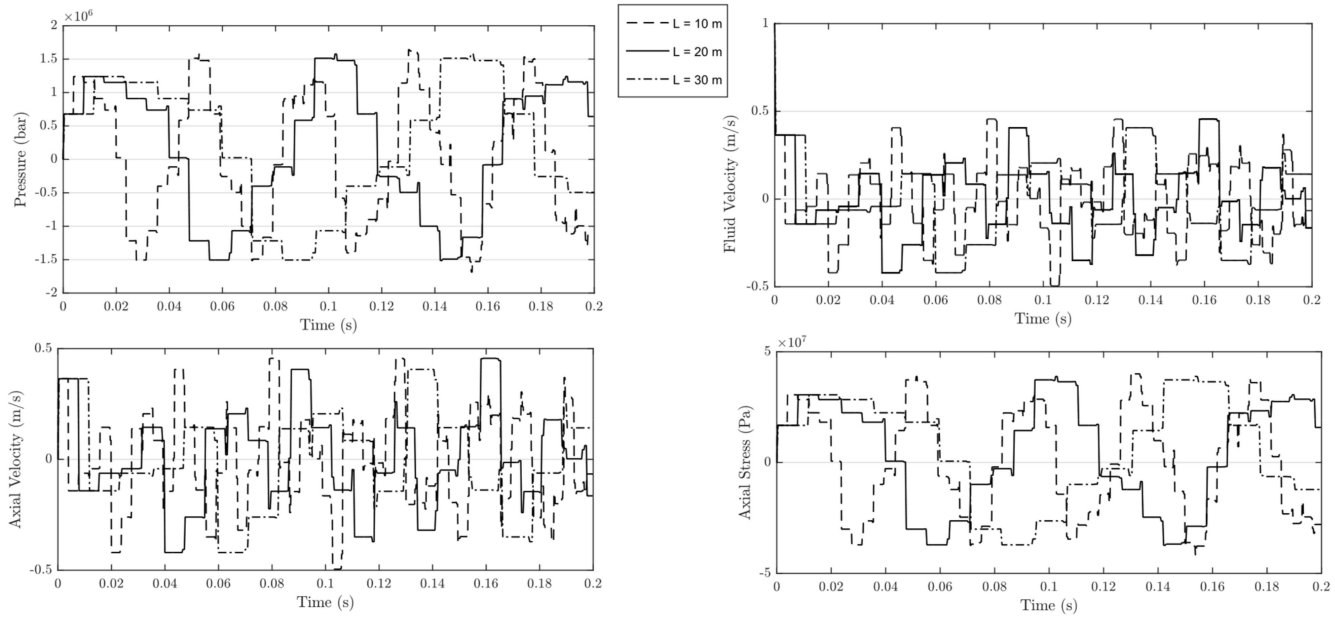

Figure 10. WH pressure, fluid flow velocity, axial tube velocity, and axial stress in the tube wall over time for the steel pipeline for pipe lengths of 10 m, 20 m, and 30 m.

The results show that the pipe length has a significant influence on the WH behavior in steel pipes. The pressure wave speed is found to be independent of the pipe length, as it is primarily determined by the properties of the fluid and the pipe material.

The magnitude of the pressure surges increases with pipe length. For the 10 m pipe, the peak pressure surge is around 1.50 MPa, while for the 30 m pipe, the peak pressure surge reaches 1.60 MPa. The longer pipe length allows the pressure wave to travel a greater distance, resulting in higher pressure amplification due to the reflection and superposition of the waves. The time taken for the pressure wave to travel from the valve to the upstream end and back to the valve increases linearly with pipe length. For the 10 m pipe, the time for the pressure wave to complete one round trip is around 0.5 ms, while, for the 30 m pipe, it is approximately 0.4 ms. The higher pressure surges in the longer pipes increase the risk of cavitation, as the pressure can drop below the vapor pressure of the fluid.

5.3. Effect of Change the Pipeline Radius

This study investigates the effect of pipe radius on the WH phenomenon with FSI in steel pipes, considering a range of pipe sizes commonly used in engineering applications. The pipe radii analyzed in this research are 300 mm, 400 mm, and 500 mm. All other dimensions and properties, including tube thickness, length, and water density, are kept constant for all materials, as specified in Table 1.

Figure 11 presents the variation of WH pressure, water flow velocity, axial tube velocity, and axial stress in the tube wall over time for the steel pipeline for pipe radii of 300 mm, 400 mm, and 500 mm.

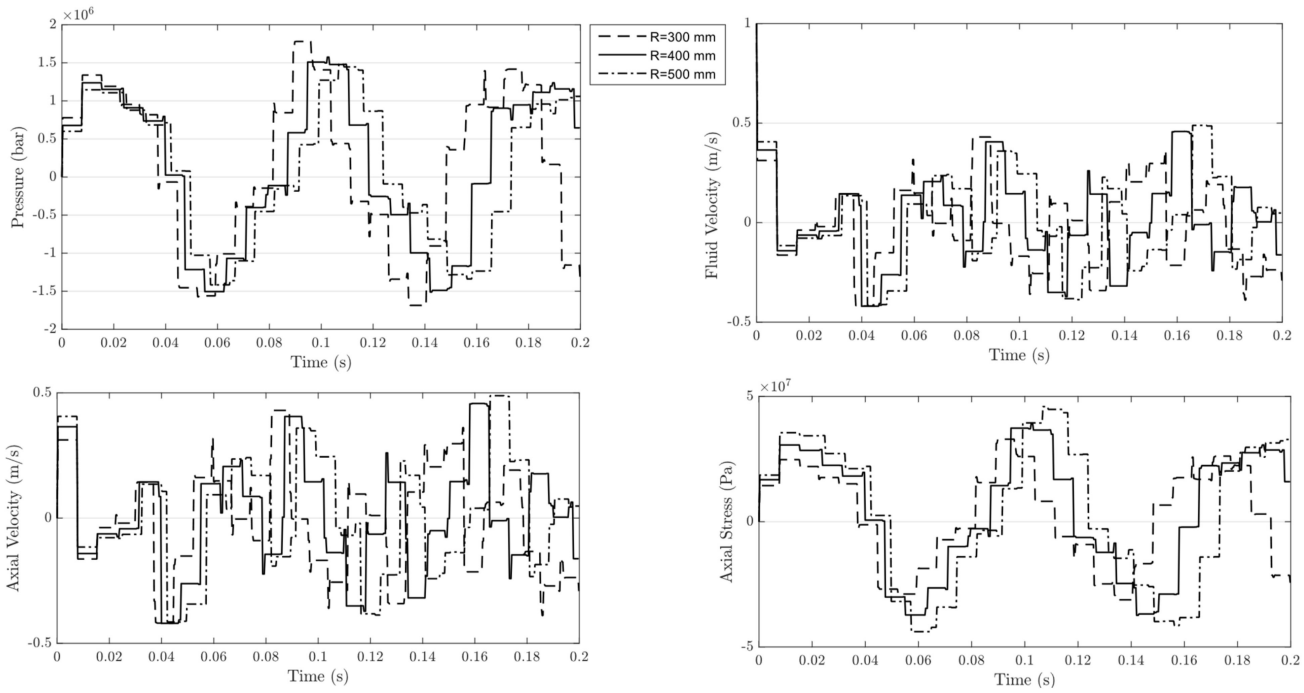

Figure 11. WH pressure, water flow velocity, axial tube velocity, and axial stress in the tube wall over time for the steel pipeline for pipe radii of 300 mm, 400 mm, and 500 mm.

The results show that the pipe radius has a significant influence on the WH behavior in steel pipes. The pressure wave speed is found to be inversely proportional to the square root of the pipe radius (refer to Equation (5)), with the 300 mm pipe having a pressure wave speed of approximately 1095 m/s, while the 500 mm pipe has a pressure wave speed of around 966 m/s. This is due to the relationship between the pressure wave speed and the effective bulk modulus of the fluid pipe system, which is affected by the pipe radius. The magnitude of the pressure surge increases with the pipe radius, with the 300 mm pipe experiencing a peak pressure surge of around 1.7 MPa, while the 500 mm

pipe reaches a peak pressure surge of 1.48 MPa. The larger pipe radius results in higher fluid inertia, leading to more severe pressure surges during the WH event. The time taken for the pressure wave to travel from the valve to the upstream end and back to the valve is independent of the pipe radius, as it is primarily determined by the pipe length and the pressure wave speed. The higher pressure surges in the larger pipes increase the risk of cavitation, as the pressure can drop below the vapor pressure of the fluid, potentially leading to the formation of vapor bubbles.

5.4. Effect of Change on Pipeline Thickness

The pipe wall thickness is another important parameter that can significantly affect the WH behavior in steel pipes.

Figure 12 presents the variation of WH pressure, water flow velocity, axial tube velocity, and axial stress in the tube wall over time for the steel pipeline for pipe thicknesses of 4 mm, 8 mm, and 12 mm. All other dimensions and properties, including tube radius, length, and water density, are kept constant for all materials, as specified in Table 1.

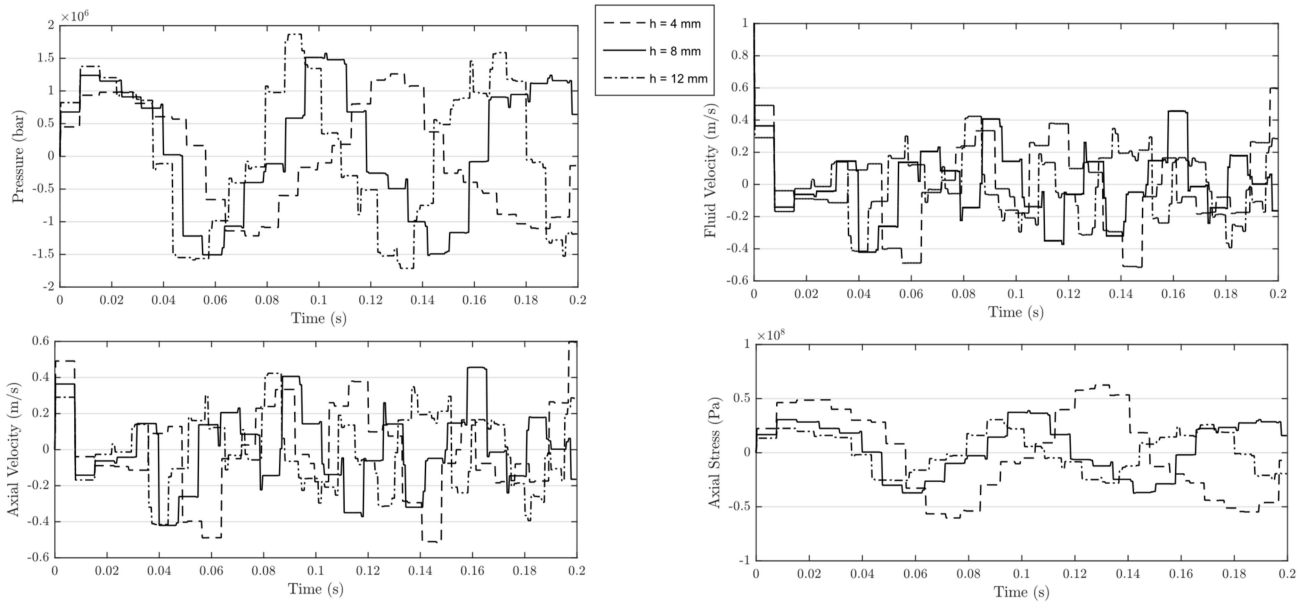

Figure 12. WH pressure, water flow velocity, axial tube velocity, and axial stress in the tube wall over time for the steel pipeline for pipe thicknesses of 4 mm, 8 mm, and 12 mm.

The pressure wave speed is proportional to the square root of the pipe wall thickness (refer to Equation (5)), with a 4 mm thick pipe having a pressure wave speed of approximately 838 m/s, while a 12 mm thick pipe has a pressure wave speed of around 1123 m/s. This is due to the relationship between the pressure wave speed and the effective bulk modulus of the fluid pipe system, which is affected by the pipe wall thickness. The magnitude of the pressure surges increases with increasing pipe wall thickness, with a 4 mm thick pipe experiencing a peak pressure surge of up to 1.25 MPa, and a 12 mm thick pipe having a peak pressure surge of around 1.75 MPa. Increasing the steel pipe wall thickness from 4 mm to 12 mm effectively reduces the magnitude of the longitudinal stress waves during a WH event. The thicker pipe walls have higher longitudinal stress wave speeds and lower peak longitudinal stresses due to their increased resistance to deformation. The reduced FSI and lower longitudinal stresses in thicker steel pipes can enhance the overall reliability and safety of the piping system under WH conditions. The wave frequency based on the wave periodic time for WH with FSI in steel pipes decreases as the pipe wall thickness increases from 4 mm to 12 mm. The thicker pipe walls result in lower pressure wave speeds, leading to longer wave periodic times and lower wave frequencies. The FSI can also influence the wave characteristics, but the general trend of decreasing frequency with increasing pipe

thickness remains. Thicker pipe walls provide more resistance to deformation, resulting in lower pressure surges during the WH event. The time taken for the pressure wave to travel from the valve to the upstream end and back to the valve is independent of the pipe wall thickness, as it is primarily determined by the pipe length and the pressure wave speed. The lower pressure surges in thicker pipes reduce the risk of cavitation.

6. Conclusions

This research aims to present the distinct outcomes for the four unknowns of FSI, which are depicted through curves illustrating the extent of the changes occurring in them, a novel aspect that has not been explored in previous research. This study also compares the responses of different parameters to WH and identifies which parameter exhibits the most significant effect. For this purpose, a numerical model has been developed. The model results provide insights into the axial stress, axial tube velocity, and water velocity, which were not readily accessible before.

The conclusions from this analysis are that the choice of pipe material significantly affects the performance of the pipeline under WH conditions. The lower pressure wave speeds and higher stress wave speeds in the PPR and GRP pipes suggest that these materials may be more suitable for applications where high-frequency vibrations are a concern. On the other hand, the higher natural frequencies of the steel pipe suggest that it may be more suitable for applications where high-frequency vibrations are not a concern.

The findings of this study demonstrate the significant impact of pipe parameters on the WH behavior in pipes. Larger pipe lengths, radii, and thicknesses are more susceptible to higher pressure surges and increased risk of cavitation, which should be considered in the design and mitigation of WH effects in fluid transport systems.

The key findings are as follows:

1. Based on the analysis, PPR and GRP show better resistance to WH than steel. Copper and ductile iron have lower resistance to WH due to the lower WH pressure and frequencies under the same operating conditions.
2. PPR is strongly recommended for use in environments where WH may occur due to its minimal susceptibility to the phenomenon.
3. In situations where WH is possible, it is advisable to choose plastic pipes because of their superior impact absorption compared with rigid materials. This helps to decrease the risk of any damage that may result from WH.
4. The pressure wave speed remains independent of pipe length, but the time for a pressure wave to complete a round trip increases with length, increasing the risk of cavitation.
5. Larger pipe radii result in higher pressure surges and fluid inertia, leading to more severe WH effects.
6. Thicker pipes have higher pressure wave speeds, peak pressure surges, and lower longitudinal stress, providing increased resistance to deformation and enhancing system reliability under WH conditions.

Author Contributions: Conceptualization, M.K., A.M.K. and T.A.E.-S.; methodology, M.K.; software, M.K. and T.A.E.-S.; validation, M.K., A.M.K. and T.A.E.-S.; formal analysis, M.K.; investigation, M.K.; writing—original draft preparation, M.K.; writing—review and editing, M.K., A.M.K. and T.A.E.-S.; supervision, A.M.K. and T.A.E.-S. All authors have read and agreed to the published version of the manuscript.

Funding: This research received no external funding.

Data Availability Statement: The original contributions presented in the study are included in the article, further inquiries can be directed to the corresponding author.

Acknowledgments: The authors would like to express their sincere gratitude to Arris Tijsseling for his invaluable help in preparing the research.

Conflicts of Interest: The authors declare no conflict of interest.

Nomenclature

Symbol	Description	Units
A_l	Cross-sectional area of liquid	m^2
A_t	Cross-sectional area of tube	m^2
a	Fluid wave speed	m/s
c	Axial stress wave speed	m/s
E	Modulus of elasticity	Pa
g	Acceleration of gravity	m/s^2
G	Shear modulus	Pa
H	Head	m
h	Tube wall thickness	m
h_f	Friction losses	m
I	Area moment of inertia	m^4
J	Polar moment of inertia	m^4
K	Water bulk modulus	Pa
L	Tube length	m
M	Moment	N.m
p	WH pressure	Pa
p_o	Pressure upstream the tank	m
Q	Water discharge	m^3/s
R	Inner radius of tube	m
t	Time	s
U	Axial tube velocity	m/s
V	Water velocity	m/s
V_r	Relative velocity	m/s
ρ_l	Density of water	kg/m^3
ρ_t	Density of tube wall	kg/m^3
σ	Axial stress in tube wall	Pa

Appendix A

Solving the Matrix Equation ($\mathbf{TB} = \Delta\mathbf{TA}$)

$$\mathbf{TB} = \Delta\ \mathbf{T}\ \mathbf{A} \tag{A1}$$

To solve this matrix equation, we begin by defining the given matrices. ($\mathbf{T}$) is the unknown matrix, while ($\mathbf{A}$) and ($\mathbf{B}$) are known square matrices, and (Δ) is a known eigenvalues diagonal matrix; see Equations (8), (9) and (13).

$$\mathbf{T} = \left[t_{ij}\right],\ \mathbf{B} = \left[b_{ij}\right],\ \mathbf{A} = \left[a_{ij}\right],\ \Delta = \mathrm{diag}(\eta_1, \eta_2, \ldots, \eta_n) \tag{A2}$$

The subsequent step involves expanding both sides of the equation, yielding a system of sixteen equations for the elements $\left(t_{ij}\right)$ of the matrix (T). These sixteen equations are then categorized into four groups, each corresponding to a row of the 4×4 matrix. This process results in a simplified matrix equation of the following form:

$$(\mathbf{B} - \eta_i\mathbf{A})\ \mathbf{t_i} = 0 \tag{A3}$$

where $\mathbf{t_i} = [\boldsymbol{t_{i1}}\boldsymbol{t_{i2}}\boldsymbol{t_{i3}}\boldsymbol{t_{i4}}]^T$.

To avoid trivial solutions where ($\mathbf{T}$) would be a zero matrix, we need to ensure that the matrix ($\mathbf{B} - \eta_i\mathbf{A}$) is singular by appropriately selecting eigenvalues (η_i). This selection is crucial to guarantee non-trivial solutions for ($\mathbf{T}$).

The eigenvalues (η_i) should be selected in accordance with Equations (25)–(28), ensuring that Equation (A2) is satisfied. Consequently, the system of Equation (A3) becomes dependent, allowing one of the four equations to be omitted in each iteration. This process is repeated for each row of equations. The resulting system of linear equations is then solved for the elements $\left(t_{ij}\right)$ in ($\mathbf{T}$). This approach ensures that the original matrix equation

($\mathbf{TB} = \Delta\mathbf{TA}$) is satisfied. For further details of the solution, refer to Tijsseling's thesis (see ref. [6]).

References

1. Riedelmeier, S. *Quantification of Fluid-Structure Interaction Effects during Water Hammer in Piping Systems*; Friedrich-Alexander-Universität Erlangen-Nürnberg (FAU): Erlangen, Germany, 2017.
2. Ferràs, D.; Manso, P.A.; Schleiss, A.J.; Covas, D.I. Fluid-structure interaction in straight pipelines: Friction coupling mechanisms. *Comput. Struct.* **2016**, *175*, 74–90. [CrossRef]
3. Weijde, P. Prediction of pressure surges and dynamic forces in pipeline systems, influence of system vibrations on pressures and dynamic forces (fluid structure interaction). In Proceedings of the Transactions of the Symposium on Pipelines, Utrecht, The Netherlands, 11–15 November 1985; pp. 327–335.
4. Walker, J.S.; Phillips, J.W. Pulse propagation in fluid-filled tubes. *J. Appl. Mech.* **1977**, *44*, 31–35. [CrossRef]
5. Stuckenbruck, S.; Wiggert, D. Unsteady flow through flexible tubing with coupled axial wall motion. In Proceedings of the 5th International Conference on Pressure Surges, Cambridge, UK, 4–6 October 1989; pp. 11–17.
6. Tijsseling, A.S. Fluid-Structure Interaction in Case of Water Hammer with Cavitation. Ph.D. Thesis, Delft University of Technology, Delft, The Netherlands, 1993.
7. Keramat, A.T.A. *Waterhammer with Column Separation, Fluid-Structure Interaction and Unsteady Friction in a Viscoelastic Pipe*; Technische Universiteit Eindhoven: Eindhoven, The Netherlands, 2012.
8. Tijsseling, A.; Lavooij, C. Waterhammer with fluid-structure interaction. *Appl. Sci. Res.* **1990**, *47*, 273–285. [CrossRef]
9. Tijsseling, A. Water hammer with fluid–structure interaction in thick-walled pipes. *Comput. Struct.* **2007**, *85*, 844–851. [CrossRef]
10. Zhang, Y.-l.; Miao, M.-f.; Ma, J.-m. Analytical study on water hammer pressure in pressurized conduits with a throttled surge chamber for slow closure. *Water Sci. Eng.* **2010**, *3*, 174–189.
11. Adamkowski, A.; Henclik, S.; Janicki, W.; Lewandowski, M. The influence of pipeline supports stiffness onto the water hammer run. *Eur. J. Mech. B/Fluids* **2017**, *61*, 297–303. [CrossRef]
12. Pezzinga, G.; Scandura, P. Unsteady flow in installations with polymeric additional pipe. *J. Hydraul. Eng.* **1995**, *121*, 802–811. [CrossRef]
13. Garg, R.K.; Kumar, A. Experimental and numerical investigations of water hammer analysis in pipeline with two different materials and their combined configuration. *Int. J. Press. Vessel. Pip.* **2020**, *188*, 104219. [CrossRef]
14. Keramat, A.; Tijsseling, A.; Hou, Q.; Ahmadi, A. Fluid–structure interaction with pipe-wall viscoelasticity during water hammer. *J. Fluids Struct.* **2012**, *28*, 434–455. [CrossRef]
15. Tijsseling, A.; Dienstverlening, W. *Fluid-Structure Interaction in Liquid-Filled Pipe Systems: Sources, Solutions and Unsolved Problems*; Report IWDE; Technische Universiteit Eindhoven: Eindhoven, The Netherlands, 2002; pp. 2–5.
16. Ferras, D.; Manso, P.A.; Schleiss, A.J.; Covas, D.I. Fluid-structure interaction in straight pipelines with different anchoring conditions. *J. Sound Vib.* **2017**, *394*, 348–365. [CrossRef]
17. Wiggert, D.; Otwell, R.; Hatfield, F. The effect of elbow restraint on pressure transients. *J. Fluids Eng.* **1985**, *107*, 298–432. [CrossRef]
18. Lavooij, C.; Tusseling, A. Fluid-structure interaction in liquid-filled piping systems. *J. Fluids Struct.* **1991**, *5*, 573–595. [CrossRef]
19. Covas, D.; Ramos, H.; Graham, N.; Maksimovic, C. The interaction between viscoelastic behaviour of the pipe-wall, unsteady friction and transient pressures. In Proceedings of the 9th International on Pressure Surges, Chester, UK, 24–26 March 2004.
20. Keramat, A.; Karney, B.; Ghidaoui, M.S.; Wang, X. Transient-based leak detection in the frequency domain considering fluid–structure interaction and viscoelasticity. *Mech. Syst. Signal Process.* **2021**, *153*, 107500. [CrossRef]
21. Gao, H.; Guo, C.; Quan, L.; Wang, S. Frequency Domain Analysis of Fluid–Structure Interaction in Aircraft Hydraulic Pipe with Complex Constraints. *Processes* **2022**, *10*, 1161. [CrossRef]
22. Li, Q.; Yang, K.; Zhang, L.; Zhang, N. Frequency domain analysis of fluid–structure interaction in liquid-filled pipe systems by transfer matrix method. *Int. J. Mech. Sci.* **2002**, *44*, 2067–2087. [CrossRef]
23. Andrade, D.M.; de Freitas Rachid, F.B.; Tijsseling, A.S. An analysis of fluid–structure interaction coupling mechanisms in liquid-filled viscoelastic pipes subject to fast transients. *J. Fluids Struct.* **2023**, *121*, 103924. [CrossRef]
24. Bayle, A.; Plouraboue, F. Laplace-Domain Fluid–Structure Interaction Solutions for Water Hammer Waves in a Pipe. *J. Hydraul. Eng.* **2024**, *150*, 04023062. [CrossRef]
25. Henclik, S. Analytical solution and numerical study on water hammer in a pipeline closed with an elastically attached valve. *J. Sound Vib.* **2018**, *417*, 245–259. [CrossRef]
26. Urbanowicz, K.; Bergant, A.; Stosiak, M.; Karpenko, M.; Bogdevičius, M. Developments in analytical wall shear stress modelling for water hammer phenomena. *J. Sound Vib.* **2023**, *562*, 117848. [CrossRef]
27. Zhang, B.; Wan, W.; Shi, M. Experimental and numerical simulation of water hammer in gravitational pipe flow with continuous air entrainment. *Water* **2018**, *10*, 928. [CrossRef]
28. Yazdi, J.; Hokmabadi, A.; JaliliGhazizadeh, M. Optimal size and placement of water hammer protective devices in water conveyance pipelines. *Water Resour. Manag.* **2019**, *33*, 569–590. [CrossRef]
29. Kim, H.; Kim, S. Two dimensional cavitation waterhammer model for a reservoir-pipeline-valve system. *J. Hydraul. Res.* **2019**, *57*, 327–336. [CrossRef]

30. Triki, A.; Chaker, M.A. Compound technique-based inline design strategy for water-hammer control in steel pressurized-piping systems. *Int. J. Press. Vessel. Pip.* **2019**, *169*, 188–203. [CrossRef]
31. Kandil, M.; Kamal, A.; El-Sayed, T. Effect of pipematerials on water hammer. *Int. J. Press. Vessel. Pip.* **2020**, *179*, 103996. [CrossRef]
32. Skalak, R. *An Extension of the Theory of Water Hammer*; Columbia University, Civil Engineering and Engineering Mechanics: New York, NY, USA, 1955.
33. Joukowsky, N. On the hydraulic hammer in water supply pipes. *Proceeding Am. Water Work. Assoc.* **1904**, *24*, 341–424.
34. Chaudhry, M.H. *Applied Hydraulic Transients*; Springer: Berlin/Heidelberg, Germany, 1979.
35. Ferras, D. Fluid-structure-interaction in pipe coils during hydraulic transients: Numerical and experimental analysis. In Proceedings of the 36th IAHR World Congress, The Hague, The Netherlands, 28 June–3 July 2015.
36. Watters, G.Z. *The Behavior of PVC Pipe Under the Action of Water Hammer Pressure Waves*; Reports Paper 20; Utah State University: Logan, UT, USA, 1971. Available online: https://digitalcommons.usu.edu/water_rep/20 (accessed on 1 April 2024).
37. Kubrak, M.; Kodura, A.; Malesińska, A.; Urbanowicz, K. Water Hammer in Steel–Plastic Pipes Connected in Series. *Water* **2022**, *14*, 3107. [CrossRef]
38. Kriaa, K.; Elgamal, M.; Farouk, M. Experimental study on reducing water hammer effects in uPVC pipes using rubber bypass tubes. *Ain Shams Eng. J.* **2023**, *15*, 102562. [CrossRef]
39. Zhang, L.; Tijsseling, A.; Vardy, A. FSI analysis of liquid-filled pipes. *J. Sound Vib.* **1999**, *224*, 69–100. [CrossRef]
40. Tijsseling, A. Exact solution of linear hyperbolic four-equation system in axial liquid-pipe vibration. *J. Fluids Struct.* **2003**, *18*, 179–196. [CrossRef]
41. Ashby, M.F.; Shercliff, H.; Cebon, D. *Materials: Engineering, Science, Processing and Design*; Butterworth-Heinemann: Oxford, UK, 2018.